because the actual masses of massive protostars are poorly determined. Our approach is to predict the properties of some well studied massive protostars in terms of their bolometric luminosities. The bolometric luminosity L_{bol} has contributions from main-sequence nuclear burning L_{ms}, deuterium burning L_D, and accretion L_{acc}. The accretion luminosity $L_{acc} = f_{acc} G m_* \dot{m}_* / r_*$, where f_{acc} is a factor of order unity accounting for energy radiated by an accretion disk, advected into the star or converted into kinetic energy of outflows, and where the stellar radius r_* may depend sensitively on the accretion rate $\dot{m}_*$. Massive stars join the main sequence during their accretion phase at a mass that also depends on the accretion rate[23]. To treat accelerating accretion rates, we have developed a simple model for protostellar evolution based on that of refs 6 and 24. The model accounts for the total energy of the protostar as it accretes and dissociates matter and, if the central temperature $T_c \gtrsim 10^6$ K, burns deuterium. We have modified this model to include additional processes, such as deuterium shell burning, and we have calibrated these modifications against the more detailed calculations of refs 23 and 25.

Our model allows us to make predictions for the masses and accretion rates of embedded protostars that are thought to power hot molecular cores (C.F.M. and J.C.T., manuscript in preparation). Figure 2 compares our theoretical tracks with the observed bolometric luminosities of several sources. We find that uncertainties in the value of the pressure create only small uncertainties in m_* for L_{bol} in excess of a few times 10^4 solar luminosities.

The infrared and submillimetre spectra of accreting protostars and their surrounding envelopes have been modelled in ref. 5, modelling the same sources shown in Fig. 2. We note that uncertainties in the structure of the gas envelope and the possible contributions from additional surrounding gas cores or diffuse gas will affect the observed spectrum. Comparing results, our inferred stellar masses are similar, but our accretion rates are systematically smaller by factors of ~2–5. The modelled[5] high accretion rates of $\sim 10^{-3} M_\odot\,\mathrm{yr}^{-1}$ for stars with $m_* \approx 10 M_\odot$ would be difficult to achieve unless the pressure was increased substantially; for example, if the stars are destined to reach $m_{*f} \approx 30 M_\odot$, pressure increases of a factor ~40 are required. □

Received 17 September 2001; accepted 2 January 2002.

1. Bernasconi, P. A. & Maeder, A. About the absence of a proper zero age main sequence for massive stars. *Astron. Astrophys.* **307,** 829–839 (1996).
2. McLaughlin, D. E. & Pudritz, R. E. Gravitational collapse and star formation in logotropic and nonisothermal spheres. *Astrophys. J.* **476,** 750–765 (1997).
3. Stahler, S. W., Palla, F. & Ho, P. T. P. in *Protostars & Planets IV* (eds Mannings, V., Boss, A. P. & Russell, S. S.) 327–351 (Univ. Arizona Press, Tucson, 2000).
4. Behrend, R. & Maeder, A. Formation of massive stars by growing accretion rate. *Astron. Astrophys.* **373,** 190–198 (2001).
5. Osorio, M., Lizano, S. & D'Alessio, P. Hot molecular cores and the formation of massive stars. *Astrophys. J.* **525,** 808–820 (1999).
6. Nakano, T., Hasegawa, T., Morino, J.-I. & Yamashita, T. Evolution of protostars accreting mass at very high rates: Is Orion IRc2 a huge protostar? *Astrophys. J.* **534,** 976–983 (2000).
7. Plume, R., Jaffe, D. T., Evans, N. J. II, Martin-Pintado, J. & Gomez-Gonzalez, J. Dense gas and star formation: Characteristics of cloud cores associated with water masers. *Astrophys. J.* **476,** 730–749 (1997).
8. Bertoldi, F. & McKee, C. F. Pressure-confined clumps in magnetized molecular clouds. *Astrophys. J.* **395,** 140–157 (1992).
9. Hillenbrand, L. A. & Hartmann, L. W. A preliminary study of the Orion nebula cluster structure and dynamics. *Astrophys. J.* **492,** 540–553 (1998).
10. van der Tak, F. F. S., van Dishoeck, E. F., Evans, N. J. II & Blake, G. A. Structure and evolution of the envelopes of deeply embedded massive young stars. *Astrophys. J.* **537,** 283–303 (2000).
11. Vázquez-Semadeni, E., Ostriker, E. C., Passot, T., Gammie, C. F. & Stone, J. M. in *Protostars & Planets IV* (eds Mannings, V., Boss, A. P. & Russell, S. S.) 3–28 (Univ. Arizona Press, Tucson, 2000).
12. Richer, J. S., Shepherd, D. S., Cabrit, S., Bachiller, R. & Churchwell, E. in *Protostars & Planets IV* (eds Mannings, V., Boss, A. P. & Russell, S. S.) 867–894 (Univ. Arizona Press, Tucson, 2000).
13. Matzner, C. D. & McKee, C. F. Efficiencies of low-mass star and star cluster formation. *Astrophys. J.* **545,** 364–378 (2000).
14. McLaughlin, D. E. & Pudritz, R. E. A model for the internal structure of molecular cloud cores. *Astrophys. J.* **469,** 194–208 (1996).
15. Larson, R. B. Turbulence and star formation in molecular clouds. *Mon. Not. R. Astron. Soc.* **194,** 809–826 (1981).
16. Stahler, S. W., Shu, F. H. & Taam, R. E. The evolution of protostars. I—Global formulation and results. *Astrophys. J.* **241,** 637–654 (1980).
17. Crutcher, R. M. Magnetic fields in molecular clouds: Observations confront theory. *Astrophys. J.* **520,** 706–713 (1999).
18. Jijina, J. & Adams, F. C. Infall collapse solutions in the inner limit: Radiation pressure and its effects on star formation. *Astrophys. J.* **462,** 874–887 (1996).
19. Shu, F. H. Self-similar collapse of isothermal spheres and star formation. *Astrophys. J.* **214,** 488–497 (1977).
20. Palla, F. & Stahler, S. W. Star formation in the Orion nebula cluster. *Astrophys. J.* **525,** 772–783 (1999).
21. Wolfire, M. G. & Cassinelli, J. Conditions for the formation of massive stars. *Astrophys. J.* **319,** 850–867 (1987).
22. Bonnell, I. A., Bate, M. R., Clarke, C. J. & Pringle, J. E. Competitive accretion in embedded stellar clusters. *Mon. Not. R. Astron. Soc.* **323,** 785–794 (2001).
23. Palla, F. & Stahler, S. W. The evolution of intermediate-mass protostars. II—Influence of the accretion flow. *Astrophys. J.* **392,** 667–677 (1992).
24. Nakano, T., Hasegawa, T. & Norman, C. The mass of a star formed in a cloud core: Theory and its application to the Orion A cloud. *Astrophys. J.* **450,** 183–195 (1995).
25. Palla, F. & Stahler, S. W. The evolution of intermediate-mass protostars. I—Basic results. *Astrophys. J.* **375,** 288–299 (1991).
26. Schaller, G., Schaerer, D., Meynet, G. & Maeder, A. New grids of stellar models from 0.8 to 120 solar masses at Z = 0.020 and Z = 0.001. *Astron. Astrophys. Suppl.* **96,** 269–331 (1992).
27. Hunter, T. R. *et al.* G34.24+0.13MM: A deeply embedded proto-B-star. *Astrophys. J.* **493,** L97–L100 (1998).
28. Molinari, S., Testi, L., Brand, J., Cesaroni, R. & Palla, F. IRAS 23385+6053: A prototype massive class 0 object. *Astrophys. J.* **505,** L39–L42 (1998).
29. Kaufman, M. J., Hollenbach, D. J. & Tielens, A. G. G. M. High-temperature molecular cores near massive stars and application to the Orion hot core. *Astrophys. J.* **497,** 276–287 (1998).
30. Wyrowski, F., Schilke, P., Walmsley, C. M. & Menten, K. M. Hot gas and dust in a protostellar cluster near W3(OH). *Astrophys. J.* **514,** L43–L46 (1999).

Acknowledgements

We thank S. Stahler, R. Pudritz, M. Walmsley and M. Krumholz for discussions. This work was supported by the NSF, by NASA (which supports the Center for Star Formation Studies) and (for J.C.T.) by a Spitzer-Cotsen fellowship from Princeton University.

Correspondence and requests for materials should be addressed to C.F.M. (e-mail: cmckee@mckee.berkeley.edu).

Coherent emission of light by thermal sources

Jean-Jacques Greffet*¶, Rémi Carminati*, Karl Joulain*, Jean-Philippe Mulet*, Stéphane Mainguy† & Yong Chen‡

** Laboratoire EM2C, CNRS, Grande Voie des Vignes, Châtenay-Malabry 92295 Cedex, France*
† CEA CESTA, Le Barp, 33114, France
‡ Laboratoire de Microstructures et de Microélectronique, CNRS, av. H. Ravera, 92220 Bagneux, France
¶ Present address: The Institute of Optics, University of Rochester, New York 14627, USA

A thermal light-emitting source, such as a black body or the incandescent filament of a light bulb, is often presented as a typical example of an incoherent source and is in marked contrast to a laser. Whereas a laser is highly monochromatic and very directional, a thermal source has a broad spectrum and is usually quasi-isotropic. However, as is the case with many systems, different behaviour can be expected on a microscopic scale. It has been shown recently[1,2] that the field emitted by a thermal source made of a polar material is enhanced by more than four orders of magnitude and is partially coherent at a distance of the order of 10 to 100 nm. Here we demonstrate that by introducing a periodic microstructure into such a polar material (SiC) a thermal infrared source can be fabricated that is coherent over large distances (many wavelengths) and radiates in well defined directions. Narrow angular emission lobes similar to antenna lobes are observed and the emission spectra of the source depends on the observation angle—the so-called Wolf effect[3,4]. The origin of the coherent emission lies in the diffraction of surface-phonon polaritons by the grating.

It is usually taken for granted that light spontaneously emitted by

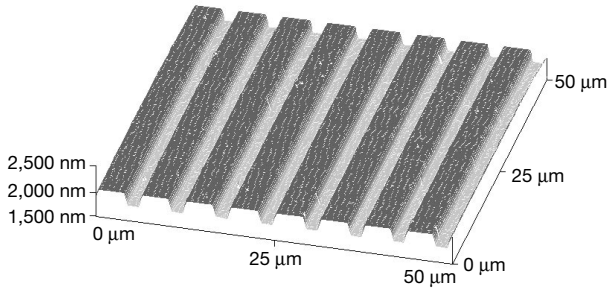

Figure 1 Image of the grating obtained by atomic force microscopy. Its period $d = 0.55\lambda$ ($\lambda = 11.36\,\mu$m) was chosen so that a surface wave propagating along the interface could be coupled to a propagating wave in the range of frequencies of interest. The depth $h = \lambda/40$ was optimized so that the peak emissivity is 1 at $\lambda = 11.36\,\mu$m. It was fabricated on SiC by standard optical lithography and reactive ion-etching techniques.

different points of a thermal source cannot interfere. In contrast, different points of an antenna emit waves that interfere constructively in particular directions producing well defined angular lobes. The intensity emitted by a thermal source is the sum of the intensities emitted by different points so that it cannot be directional. However, it has been shown[1,2] recently that some planar sources may have a spectral coherence length in the plane much larger than a wavelength and can be quasi-monochromatic in the near-field. This paves the way for the construction of a thermal source that could radiate light within narrow angular lobes as an antenna instead of having the usual quasi-lambertian angular behaviour.

Here we report experimental measurements demonstrating that it is possible to build an infrared antenna by properly designing a periodic microstructure on a polar material. Such an antenna radiates infrared light in a narrow solid angle when it is heated. Another unusual property of this source is that its emission spectrum depends on the observation direction. This property was first predicted by Wolf as a consequence of spatial correlations for random sources[3,4]. This effect has been demonstrated experimentally for artificial secondary sources[4,5] but has never been observed for direct thermal emission. In addition, the emissivity of the source is enhanced by a factor of 20 compared to the emissivity of a flat surface.

Using theories developed recently[6] to interpret the emission data by gratings, we have designed and optimized a periodic surface profile that produces a strong peak of the emissivity around a wavelength $\lambda = 11.36\,\mu$m. The grating (see Fig. 1) has been ruled on a SiC substrate. A similar grating of doped silicon with very deep depths has been investigated[7]. The authors attributed the particular properties observed to organ pipe modes in the microstructure[7]. However, the role of coherence induced by surface waves and the exact mechanism were not understood at that time[2,6].

The measurements of the thermal emission in a plane perpendicular to the lines of the grating are shown in Fig. 2. Emission is highly directional and looks very similar to the angular pattern of an antenna. We have also plotted (see Fig. 2) the calculated emission pattern. The qualitative discussion of the introduction suggests that the small angular width of the emission pattern is a signature of the local spatial coherence of the source. A proof of this stems from the fact that the source has a width $L = 5$ mm and a spectral coherence length $l \ll L$ and that its temperature is uniform. Hence, we can assume that the source is a quasi-homogeneous source[8]. With this assumption, it is known that the radiant intensity and the spectral degree of coherence in the plane of the source are related by a Fourier transform relationship[8]. Therefore, the angular width θ of the lobe emission varies qualitatively with λ/l for this locally coherent source instead of with λ/L, as for a globally coherent source. Thus a small angular aperture of the far-field radiation is the signature of a spectral coherence length in the source much larger than the wavelength. To overcome the experimental resolution limit of our direct emissivity measurement, we measured the reflectivity R. From Kirchhoff's law[9], we know that the polarized directional spectral emissivity ϵ is given by $\epsilon = \alpha = 1 - R$ where α is the absorptivity and R is the reflectivity of the grating. Results are plotted in Fig. 3. There is a remarkable quantitative agreement between the data taken at room temperature and theoretical calculations. We note that the peak at 60° has an angular width θ as narrow as 1° so that the corresponding spectral coherence length is as large as $\lambda/\theta \approx 60\lambda \approx 0.6$ mm. This suggests that a thermal source with a size L on the order of the spectral coherence length l, namely a globally coherent thermal source, could be achieved.

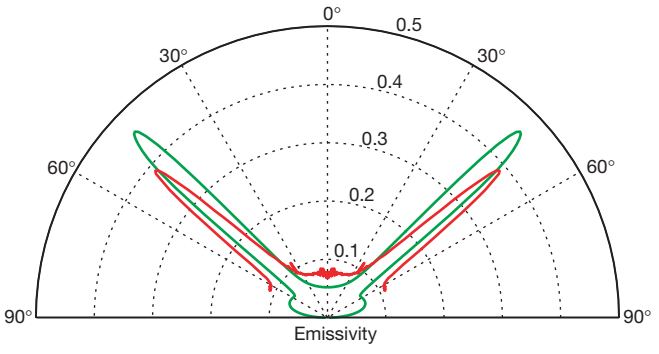

Figure 2 Polar plot of the emissivity of the grating depicted in Fig. 1 at $\lambda = 11.36\,\mu$m and for *p*-polarization. Red, experimental data; green, theoretical calculation. The measurements were taken by detecting the intensity emitted by the sample in the far field as a function of the emission angle. A HgCdTe detector placed at the focal length of a ZnSe lens was used. The sample was mounted on a rotation stage. The theoretical result was obtained by computing the reflectivity of the sample and using Kirchhoff's law ($\epsilon = \alpha = 1 - R$). To fit the data, we took into account the spectral resolution (0.22 μm) and the angular resolution (3°) of the measurements. The disagreement is due to the fact that for the calculation, the index at room temperature is used whereas emission data were taken with a sample in a local thermal equilibrium situation at a temperature of 773 K. Comparison between the two curves illustrates the validity of Kirchhoff's law for polarized monochromatic directional quantities. The surrounding medium was at 300 K and the background signal was subtracted. The emissivity for *s*-polarization (not shown) does not show any peak and is very close to its value for a flat surface. Note that most of the emitted light is emitted in the narrow lobe (that is, coherently).

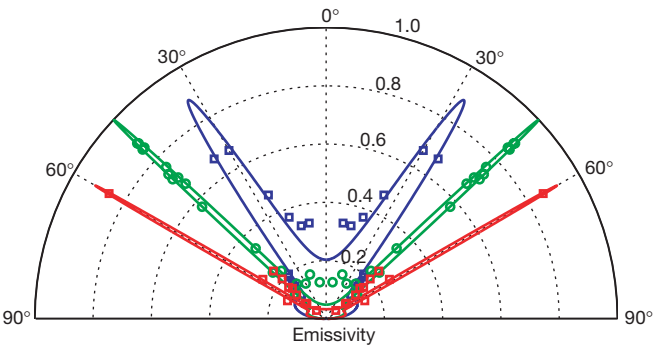

Figure 3 Emissivity of a SiC grating in *p*-polarization. Blue, $\lambda = 11.04\,\mu$m; red, $\lambda = 11.36\,\mu$m; green, $\lambda = 11.86\,\mu$m. The emissivity was deduced from measurements of the specular reflectivity R using Kirchhoff's law. The data have been taken at ambient temperature using a Fourier transform infrared (FTIR) spectrometer as a source and a detector mounted on a rotating arm. The angular acceptance of the spectrometer was reduced to a value lower than the angular width of the dip. The experimental data are indicated by circles; the lines show the theoretical results. An excellent agreement is obtained when the data are taken at ambient temperature, which supports our interpretation of the slight disagreement in Fig. 1 being due to the variation of index with temperature.

A surprising property of the emissivity patterns of Fig. 3 is that they depend strongly on the wavelength. This suggests that the emission spectra depend on the emission direction. This would be a manifestation of the Wolf effect[3,4]. To observe this effect, we have taken several spectra of the reflectivity of the surface at different angles. Fig. 4 shows experimental and theoretical spectra for different observation angles. The position of the peaks of emissivity (dips of reflectivity) depends strongly on the observation angle. It is important to emphasize that this property is not merely a scattering effect but is a consequence of the partial spatial coherence of the source. The value of the reflectivity is also remarkable. By ruling a grating onto a material which is essentially a mirror, we were able to produce a perfect absorber. This behaviour has already been observed for metallic gratings and attributed to the resonant excitation of surface plasmons. This is the first time, to our knowledge, that total absorption in the infrared owing to excitation of surface-phonon polaritons has been reported.

In order to prove experimentally the role of the surface wave, we have done spectral measurements of the emissivity for *s*- and *p*-polarization. The peaks are never observed for *s*-polarization nor for *p*-polarization in the spectral region where surface waves cannot exist. In order to characterize quantitatively the role of the surface waves, we have obtained the dispersion relation from reflectivity measurements[6]. The results are displayed in Fig. 5 and compared with theory. We note that the interaction of the surface wave with the grating produces the aperture of a gap close to the band edge. Figure 5 shows that our experiment allows us to directly see surface-phonon polaritons. It also yields additional insight into the Wolf-effect[3,4] mechanism. Emission of infrared light has already been used to study surface excitations, but using prisms to couple the surface waves to propagating modes[10].

We now discuss the physical origin of coherent thermal emission. We wish to understand how random thermal motion can generate a coherent current along the interface. The key lies in the coherent properties of surface waves (either surface-plasmon polaritons or surface-phonon polaritons) demonstrated in refs 1 and 2. Both are mechanical delocalized collective excitations involving charges. Surface-phonon polaritons are phonons in a polar material, whereas surface-plasmon polaritons are acoustical-type waves in an electron gas. In both cases, these waves have the following two properties: (1) they are mechanical modes of the system that can be resonantly excited; (2) they are charge-density waves, that is, they generate electromagnetic fields. Because these excitations are delocalized, so are the corresponding electromagnetic fields.

From a classical point of view, each volume element of the thermal source can be modelled by a random point-like source that excites an extended mode: the surface wave. This is similar to some extent to the emission of sound by a string of a piano. The source is a hammer that strikes the string at a particular point. Then the modes of the string are excited producing a vibration along the full length of the string. At that point of the analogy, as anyone can hear the vibrations of a piano string, we may wonder why the coherent electromagnetic surface waves are not usually observed. The reason is that surface modes have a wavevector larger than $2\pi/\lambda$ so that they are evanescent. Their effect is not seen in the far-field.

However, by ruling a grating on the interface, we are able to couple these surface modes to propagating modes. The relationship between the emission angle θ and the wavelength λ is simply given by the usual grating law

$$\frac{2\pi}{\lambda}\sin\theta = k_{\parallel} + p\frac{2\pi}{d}$$

where p is an integer and $k_{\parallel}$ is the wavevector of the surface wave. Thus, by modifying the characteristics of the surface profile, it is possible to modify the direction and the value of the emissivity of the surface at a given wavelength. It is also possible to modify the emission spectrum in a given direction. Such gratings can be used to design infrared sources with specific properties.

This may also have interesting applications such as modifying the radiative heat transfer for a given material. Indeed, we have demonstrated that a reflectivity of 94% can be reduced to almost zero in the infrared for SiC. This could also be done for glass, which

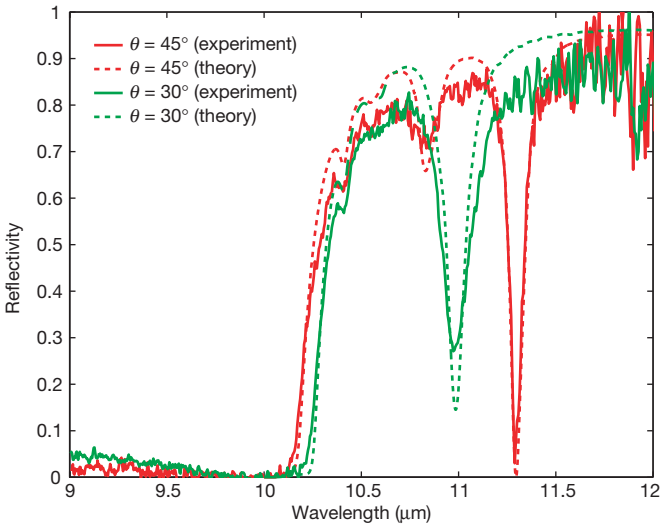

Figure 4 Comparison between measured and calculated spectral reflectivities of a SiC grating at room temperature. The incident light is *p*-polarized. The dip observed at 45° and $\lambda = 11.36\ \mu$m coincides with the emission peak observed in Figs 2 and 3. The figure shows clearly that the reflectivity spectra depend on the observation angle. Using Kirchhoff's law, it follows that the emission spectra depend on the observation angle. This is a manifestation of the Wolf effect[3,4].

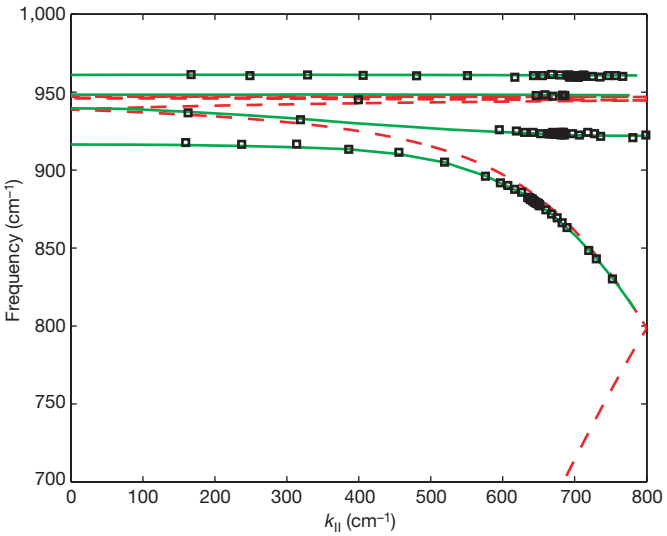

Figure 5 Dispersion relation wavevector, $\omega(k_{\parallel})$, of surface-phonon polaritons. Data points, experimental dispersion relation. Solid green curve, theoretical dispersion relation for the grating. Dotted red curve, theoretical dispersion relation for the flat surface. This figure explains the mechanism of the Wolf effect[3,4] for this particular source. The spatial coherence in the plane of the source is due to the presence of a surface wave. For a fixed frequency ω, it can be seen that there is only one possible wavevector $k_{\parallel}(\omega)$. Thus the spectral degree of coherence at ω oscillates[2] with a particular wavelength $2\pi/k_{\parallel}(\omega)$. When observing in the far field at an angle θ such that $ck_{\parallel}(\omega)/\omega = \sin\theta$ there is a strong contribution of the surface wave at frequency ω. By varying the observation angle, the frequency varies according to the dispersion relation of the surface wave. It is seen that the strong Wolf effect produced by this source is due to (1) the thermal excitation of surface waves which produce the spatial coherence and (2) the propagation in vacuum which selects one particular wavevector.

is a polar material that has a large reflectivity in the infrared owing to the presence of resonances. This would allow us to increase the radiative cooling of the material if the emission is enhanced in a region where absorption is low, because the atmosphere does not emit. Another promising application of our results is the possibility of modifying the heat transfer in the near-field. Materials that are separated by distances smaller than the typical wavelength exchange radiative energy through evanescent waves. When surface waves are resonantly excited, they provide the leading contribution[11]. Thus, the heat transfer is almost monochromatic. This may be used to enhance the efficiency of infrared photovoltaic cells[12]. □

Received 25 June; accepted 20 December 2001.

1. Shchegrov, A., Joulain, K., Carminati, R. & Greffet, J. J. Near-field spectral effects due to electromagnetic surface excitations. *Phys. Rev. Lett.* **85,** 1548–1551 (2000).
2. Carminati, R. & Greffet, J. J. Near-field effects in spatial coherence of thermal sources. *Phys. Rev. Lett.* **82,** 1660–1663 (1999).
3. Wolf, E. Non-cosmological red-shifts of spectral lines. *Nature* **326,** 363–365 (1987).
4. Wolf, E. & James, D. F. Correlation-induced spectral changes. *Rep. Prog. Phys.* **59,** 771–818 (1996).
5. Morris, G. M. & Faklis, D. Effects of source correlation on the spectrum of light. *Opt. Commun.* **62,** 5–11 (1987).
6. Le Gall, J., Olivier, M. & Greffet, J. J. Experimental and theoretical study of reflection and coherent thermal emission by a Sic grating supporting a surface photon polariton. *Phys. Rev. B* **55,** 10105–10114 (1997).
7. Hesketh, P. J., Zemel, J. N. & Gebhart, B. Organ pipe radiant modes of periodic micromachined silicon surfaces. *Nature* **325,** 549–551 (1986).
8. Mandel, L. & Wolf, E. *Optical Coherence and Quantum Optics.* Sec. 5.3 (Cambridge Univ. Press, New York, 1995).
9. Greffet, J. J. & Nieto-Vesperinas, M. Field theory for the generalized bidirectional reflectivity: derivation of Helmholtz's reciprocity principle and Kirchhoff's law. *J. Opt. Soc. Am. A* **10,** 2735–2744 (1998).
10. Zhizhin, G. N., Vinogradov, E. A., Moskalova, M. A. & Yakovlev, V. A. Applications of surface polaritons for vibrational spectroscopic studies of thin and very thin films. *Appl. Spectrosc. Rev.* **18,** 171–263 (1982).
11. Mulet, J. P., Joulain, K., Carminati, R. & Greffet, J. J. Nanoscale radiative heat transfer between a small particle and a plane surface. *Appl. Phys. Lett.* **78,** 2931–2933 (2001).
12. Whale, M. D. in *Proc. Conf. on 'Heat Transfer and Transport Phenomena in Microscale'* (ed. Celata, G. P.) 339–346 (Begell House, New York, 2000).

Competing interests statement

The authors declare that they have no competing financial interests.

Correspondence and requests for materials should be addressed to J.-J.G. (e-mail: greffet@em2c.ecp.fr).

A general process for *in situ* formation of functional surface layers on ceramics

Toshihiro Ishikawa, Hiroyuki Yamaoka, Yoshikatsu Harada, Teruaki Fujii & Toshio Nagasawa

Ube Research Laboratory, Corporate Research & Development, Ube Industries Ltd, 1978-5 Kogushi, Ube City, Yamaguchi 755-8633, Japan

Ceramics are often prepared with surface layers of different composition from the bulk[1,2], in order to impart a specific functionality to the surface or to act as a protective layer for the bulk material[3,4]. Here we describe a general process by which functional surface layers with a nanometre-scale compositional gradient can be readily formed during the production of bulk ceramic components. The basis of our approach is to incorporate selected low-molecular-mass additives into either the precursor polymer from which the ceramic forms, or the binder polymer used to prepare bulk components from ceramic powders. Thermal treatment of the resulting bodies leads to controlled phase separation ('bleed out') of the additives, analogous to the normally undesirable outward loss of low-molecular-mass components from some plastics[5–9]; subsequent calcination stabilizes the compositionally changed surface region, generating a functional surface layer. This approach is applicable to a wide range of materials and morphologies, and should find use in catalysts, composites and environmental barrier coatings.

To avoid the concentration of thermomechanical stress at the interface between the surface layer and the bulk material, many materials have been developed that have gradually varying properties as the distance into the material increases[10]. Such materials can contain gradients in morphology or in composition. Gradients in morphology can, for example, result in materials that have a graded distribution of pore sizes on a monolith of silica aerogel, and a type of integral plastic. These materials have been created by strictly controlling the vaporization of the volatile during the production process[11,12]. Gradients in chemical composition have been achieved, for example: (1) chemical vapour deposition[13,14], (2) powder methods such as slip cast or dry processing[15], (3) various coating methods[16], and (4) thermal chemical reaction[2,17]. Of these, (1) and (4) are relatively expensive, complicated and result in damage to bulk substrates. (2) and (3) produce stepped gradient structures, and it is difficult to control the thickness of each layer to less than 100 nm. Furthermore, most of these processes are not easily adapted to coating samples in the form of fibre bundles, fine powders or other materials with complicated shapes.

We have addressed the issue of establishing an inexpensive and widely applicable process for creating a material with a compositional gradient and excellent functionality. A schematic representative of our new *in situ* formation process for functional surface layers, which have a gradient-like structure towards the surface, is shown in Fig. 1. The important feature of our method is that the surface layer of the ceramic is not deposited on the substrate, but is formed during the production of the bulk ceramic. We confirmed that our process is applicable to any type of system as long as, in the green-body (that is, not-calcined) state, the system contains a resin and a low-molecular-mass additive that can be converted into a functional ceramic at high temperatures. Here, the resin is a type of precursor polymer (polycarbosilane, polycarbosilazane, polysilastyrene, methylchloropolysilane, and so on) or binder polymer used for preparing green bodies from ceramic powders[18]. Although the former case (using precursor polymers) is explained in detail in this Letter, the latter case using binder polymers was also confirmed by treating a Si_3N_4 body with a TiN surface layer. Si_3N_4 can exhibit excellent thermal stability and wear resistance in the high-speed machining of cast iron, but shows poor chemical wear resistance in the machining of steel[19]. In order to avoid this problem, TiN coating, by means of expensive chemical vapour deposition, has often been performed on previously prepared Si_3N_4 substrates. But if our process is appropriately applied, formation of the TiN surface layer could be achieved during the sintering process of the Si_3N_4 green body. In this case, titanium(IV) butoxide and polystyrene are used as the low-molecular-mass additive and binder polymer, respectively. By a combination of sufficient maturation (in air at 100 °C) and subsequent sintering (in NH_3+H_2+N_2 at 1,200 °C), Si_3N_4 covered with TiN is successfully produced. This technology would be very useful for producing ceramic materials with complicated shapes and various coating layers. Moreover, our process is advantageous for preparing precursor ceramics (particularly fine particles, thin fibrous ceramics and films). The systems to which our concept is applicable are shown in Fig. 1.

Here we give a detailed account of the results for the precursor ceramic obtained using polycarbosilane. Polycarbosilane $(-SiH(CH_3)-CH_2-)_n$ is a representative pre-ceramic polymer for preparing SiC ceramics—for example, Hi-Nicalon fibre[20] and Tyranno SA fibre[21]. Furthermore, oxide or nitride can also be produced from the polycarbosilane by firing in air or ammonia, respectively. Our new technology makes full use of the bleed-out